Sensors and Actuators A 165 (2011) 35–42

Contents lists available at ScienceDirect

Sensors and Actuators A: Physical

journal homepage: www.elsevier.com/locate/sna

Micromachined gyroscope concept allowing interchangeable operation in both robust and precision modes

Adam R. Schofield*, Alexander A. Trusov, Andrei M. Shkel

MicroSystems Laboratory, Department of Mechanical and Aerospace Engineering, University of California, Irvine, 4200 Engineering Gateway, Irvine, CA 92697, USA

ARTICLE INFO

Article history:
Available online 1 June 2010

Keywords:
MEMS
Vibratory gyroscopes
Mode-matching
Robustness

ABSTRACT

This paper presents a new gyroscope design concept with a multi-degree of freedom (DOF) sense mode enabling interchangeable operation in robust or precision modes. This is accomplished using a complete 2-DOF coupled system which, unlike previous multi-DOF designs based on dynamic vibration absorbers, allows for the specification of the sense mode resonances and coupling between the masses independent of operational frequency. The robust mode corresponds to operation between the 2-DOF sense mode resonant peaks providing a response gain and bandwidth controlled at the design level by frequency spacing; the precision mode, however, relies on mode-matching the drive to one of the sense mode resonant frequencies where larger response gains are achieved through vacuum operation. The complete 2-DOF sense mode provides the gyroscope with distinct advantages over similar devices based on 1-DOF systems: the robust mode introduces a gain advantage versus conventional mismatched operation, while the precision mode gain-bandwidth is larger for the same pressures. Experimental rate characterization of a silicon-on-insulator prototype in air for both robust and precision modes demonstrated scale factors of 0.282 and 0.690 mV/°/s, respectively, while the scale factor improvement due to precision mode operation is projected to increase by 40 dB for operation in 1 mTorr vacuum.

1. Introduction

Coriolis vibratory gyroscopes operate based on a transfer of energy between the drive and sense modes in the presence of an input angular rate [1]. In its conventional micromachined form, these modes are realized as single degree of freedom (DOF) dynamic systems, each having their own distinct resonant frequency based on the structural design. The operational method of the gyroscope, and ultimately its performance, is determined by the relative positioning of these two modes. Mode-matched operation, typically reserved for applications requiring high resolution, is achieved by setting the drive and sense resonant frequencies to be equal; this allows the sensor output to be increased proportionally to the sense mode quality factor, yielding higher sensitivities at the cost of reduced bandwidth and robustness [2]. Separating the resonant frequencies by some prescribed amount, or mode-mismatching, is more common in commercial devices as it provides increased robustness (at the cost of reduced sensitivity) [3–5]. This is because the stability of the output over a broad temperature range is critical for automotive and consumer electronics applications [6–9].

Previously, new gyroscope design concepts were introduced aimed at robust operation using an expanded sense mode mechanical design space through increased degrees of freedom [10–12]. Unlike conventional devices [13,14], the multi-DOF designs utilized two coupled sense masses in the sense mode forming a 2-DOF dynamic system with two resonant frequencies and a wide region of constant amplitude between them. While the gain and the bandwidth of this operational region is controlled solely by the resonant frequency spacing, a constraint limited the minimal achievable spacings as the operational frequency was increased with a fixed device size [15]. This is a direct effect of the incomplete 2-DOF design space consisting of only two suspensions which eliminates the ability to independently define the frequency spacing and the coupling between the masses.

In contrast, a complete 2-DOF system consisting of two masses and three suspensions alleviates this issue allowing for the arbitrary specification of frequency spacing independent of operational frequency; implementing such a system as a physical layout, however, poses a significant design challenge. Multi-DOF gyroscopes utilizing complete 2-DOF sense modes have been previously demonstrated in [16,17]. Both devices were based on symmetrically decoupled layouts [18] which required the use of bidirectional flexures while also mandating specific suspension designs for the automatic positioning of the drive mode between the sense modes

* Corresponding author.
E-mail address: adam@adamschofield.com (A.R. Schofield).

0924-4247/$ – see front matter © 2010 Elsevier B.V. All rights reserved.
doi:10.1016/j.sna.2010.04.015

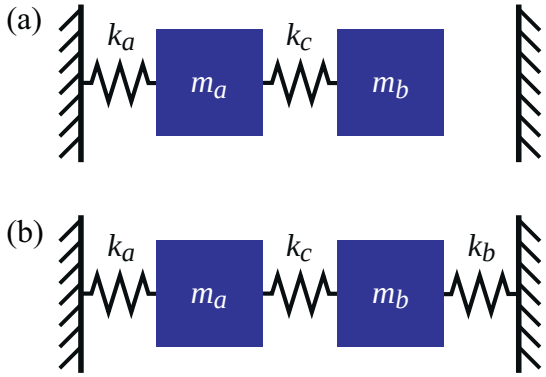

Fig. 1. The two different types of 2-DOF coupled sense mode systems. (a) Dynamic vibration absorber type 2-DOF system. (b) Complete, fully coupled 2-DOF system.

resonances [16] and the maximization of the coupled system amplitude ratio [17].

Recently, a new micromachined gyroscope design was introduced which takes advantage of a complete 2-DOF sense mode dynamic system through the use of a second, inner decoupling frame [19,20]. The proposed design maintains x–y symmetry while also eliminating the need for bidirectional suspensions. Furthermore, the complete control of the 2-DOF sense mode dynamic system enables a new operational method where the drive mode can be interchangeably placed between the sense mode peaks (robust mode) or mode-matched to one of the resonant peaks (precision mode). Since the design concept allows full control over the amount of coupling between the masses, the sense mode frequency response can be tailored for specific applications.

In this paper, a detailed description, analysis, and characterization of the newly introduced gyroscope concept is presented. Section 2 includes a comparison of the complete 2-DOF system to the dynamic vibration absorber used previously, a presentation of the proposed structural schematic, and the derivation of sense mode design equations in terms of physical parameters. Next, Section 3 introduces the method of interchangeable operation followed by a presentation of the complete 2-DOF system advantages over similar 1-DOF sense mode devices. An experimental characterization of the new device is presented in Section 4 which demonstrates angular rate operation of both the robust and precision modes using a silicon-on-insulator (SOI) prototype. Finally, Section 5 concludes the paper with a summary of results.

2. Complete multi-DOF sense mode gyroscope design concept

This section introduces the proposed gyroscope design concept which takes advantage of a complete 2-DOF sense mode. The key differences between previous multi-DOF systems and the one utilized in this work are highlighted in Section 2.1 followed by a description of the structural layout, Section 2.2, and derivation of sense mode design equations, Section 2.3.

2.1. DVA versus fully coupled sense mode

Conceptual diagrams of a dynamic vibration absorber (DVA), used in [10–12], and a complete, fully coupled 2-DOF dynamic system proposed for this work are presented in Fig. 1. The DVA is characterized by two masses, m_a and m_b, and only two suspension elements, k_a and k_c. The structural frequencies for this coupled system can be formulated as,

$$\omega_a^2 = \frac{k_a + k_c}{m_a}, \quad \omega_b^2 = \frac{k_c}{m_b}, \quad \omega_c^2 = \frac{k_c}{\sqrt{m_a m_b}}, \tag{1}$$

where ω_a and ω_b are the frequencies of the system if the larger mass m_a and the smaller mass m_b from Fig. 1(a) are held clamped, respectively, while ω_c is a term that expresses the strength of the coupling between the two masses [21].

An examination of Eq. (1) reveals that the three terms are not independent of each other, but rather a dependence exists between ω_b and ω_c,

$$\omega_c^2 = \mu\omega_b^2, \tag{2}$$

where the proportionality constant, μ, is related to the mass ratio of the system, defined as $\mu^2 = m_b/m_a$. This means that the structural frequency of mass m_b and the amount of coupling between the masses cannot be defined independently, giving rise to the frequency scaling issues discussed in [15].

In order to alleviate the frequency scaling constraints of DVA type sense modes, a complete, fully coupled 2-DOF coupled system, Fig. 1(b), is proposed. This system is comprised of two masses, m_a and m_b, and three suspension elements, k_a, k_b, and k_c. The structural frequencies of a complete, 2-DOF dynamic system can be formulated as,

$$\omega_a^2 = \frac{k_a + k_c}{m_a}, \quad \omega_b^2 = \frac{k_b + k_c}{m_b}, \quad \omega_c^2 = \frac{k_c}{\sqrt{m_a m_b}}, \tag{3}$$

where ω_a and ω_b are again the uncoupled frequencies of m_a and m_b while ω_c expresses the strength of the coupling [21]. When the values in Eqs. (1) and (3) are compared, it can clearly be seen that the addition of the third suspension eliminates the dependence of ω_b and ω_c that exists for DVA-based systems. Thus, a sense mode which utilizes a complete, three suspension 2-DOF dynamic system enables the specification of the structural frequencies and amount of coupling independent of each other, overcoming a limitation of previous designs.

2.2. Structural design

While a complete 2-DOF sense mode was conceptually shown to alleviate the frequency scaling issues related to dynamic vibration absorber systems, implementing it as the sense mode of a gyroscope is not a trivial problem. The approach taken in this work is illustrated by the lumped structural schematic of the new gyroscope concept in Fig. 2(a). The design, like previous multi-DOF sense mode devices, consists of a conventional drive mode that is mechanically decoupled from a 2-DOF sense mode dynamic system formed by the two coupled sense masses, m_a and m_b. The major difference between the current work and previous multi-DOF implementations [10–12,16,17], however, is the addition of a second, inner decoupling frame that connects the smaller sense mass m_b to a central anchor. The use of this second decoupling frame enables the inclusion of a third suspension element, k_b, thereby allowing the realization of a complete 2-DOF sense mode without the need for a bidirectional flexure.

Implementing a fully coupled sense mode using a second, inner frame and a central anchor acts to preserve x–y symmetry of the design while also maintaining the mass-in-frame decoupling used in previous multi-DOF devices. This can be seen in the physical layout schematic of the proposed multi-DOF sense mode gyroscope, Fig. 2(b); the smaller mass m_b is contained completely within and connected to the larger mass m_a with k_c, while the outer and inner frames provide connections for the k_a and k_b suspensions, respectively, to the fixed anchors. Thus, a complete, frame-decoupled, x–y symmetric 2-DOF sense mode with three suspensions can be realized as a micromachined implementation eliminating the detrimental frequency scaling effects of dynamic vibration absorbers.

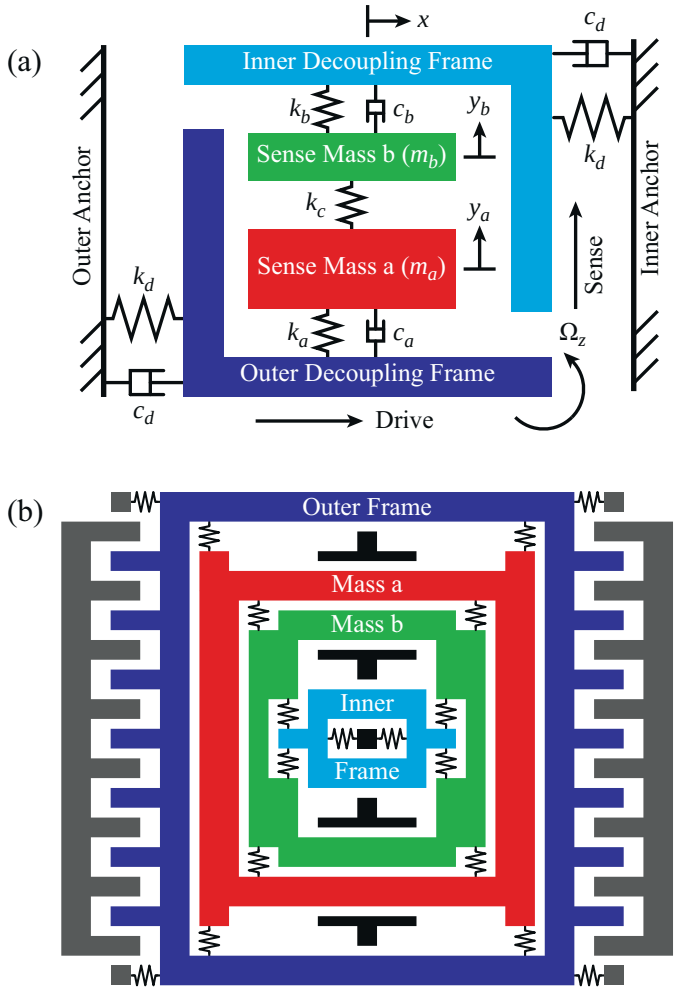

Fig. 2. Lumped structural models of the complete 2-DOF sense mode gyroscope concept. (a) Structural schematic of the gyroscope concept. (b) Physical layout schematic of the gyroscope concept highlighting the mass-in-frame decoupling approach.

2.3. Sense mode design equations

As illustrated by Fig. 2 above, the complete 2-DOF sense mode enables the specification of the sense mode resonant frequencies and amount of coupling between the masses independent of the operational frequency. This is due to the mass-in-frame decoupling used where the drive mode natural frequency, ω_d, can be obtained independent of the sense mode parameters through adjustment of either the suspensions, k_d, or the frame masses. The sense mode natural frequencies, on the other hand, are determined using the 2-DOF eigenvalue equation,

$$\omega^4 - \omega^2(\omega_a^2 + \omega_b^2) + (\omega_a^2\omega_b^2 - \omega_c^4) = 0, \tag{4}$$

which has the following solutions,

$$\omega_{1,2}^2 = \frac{1}{2}(\omega_a^2 + \omega_b^2 \mp \sqrt{\omega_a^4 + \omega_b^4 - 2\omega_a^2\omega_b^2 + 4\omega_c^4}), \tag{5}$$

where $\omega_{1,2}$ are the desired lower and higher sense mode resonances in terms of the structural frequencies defined in Eq. (3).

While the drive and sense modes are structurally independent from each other, the relative positioning of the frequencies is critical for operation of the gyroscope. For the following analysis, the natural frequency of the drive is assumed to be equally spaced from the two sense resonant peaks. This means that the desired sense mode resonances can be expressed as,

$$\omega_{1,2} = \omega_d \mp \frac{\Delta}{2}, \tag{6}$$

in terms of the sense mode peak spacing, $\Delta = \omega_2 - \omega_1$. Substituting Eq. (6) into Eq. (5) and solving for the structural frequencies gives,

$$\omega_{a,b}^2 = \omega_d^2 + \left(\frac{\Delta}{2}\right)^2 \pm \sqrt{\omega_d^2\Delta^2 - \omega_c^4}, \tag{7}$$

which are the sense mode design equations for the structural parameters required to achieve the desired 2-DOF sense mode resonant frequencies.

The difference between the DVA design equations derived in [15] and Eq. (7) is the freedom to specify the amount of coupling, through adjustment of ω_c, independent of the desired sense mode frequencies, $\omega_{1,2}$. The presence of a square root term, however, implies that the amount of coupling must be within a limited range in order to result in a physically realizable system. Therefore, it is easier to express the coupling in terms of a percentage of the maximum,

$$\omega_c^2 = \varepsilon\omega_d\Delta, \quad \text{where} \quad 0 < \varepsilon < 1, \tag{8}$$

using a coupling parameter, ε. Substituting Eq. (8) into Eq. (7) gives

$$\omega_{a,b}^2 = \omega_d^2 + \left(\frac{\Delta}{2}\right)^2 \pm \omega_d\Delta\sqrt{1-\varepsilon^2}, \tag{9}$$

which are the sense mode design equations in terms of desired operational frequency, ω_d, sense mode resonant frequency spacing, Δ, and the amount of coupling, ε. Using Eq. (3) and (8), the stiffnesses required to achieve the desired sense mode resonant frequencies can be found from the following,

$$k_a = \omega_a^2 m_a - k_c,$$

$$k_b = \omega_b^2 m_b - k_c,$$

$$k_c = \varepsilon\omega_d\Delta\sqrt{m_a m_b},$$

where $\omega_{a,b}$ is given by Eq. (9) assuming the value of the masses are known.

3. Interchangeable operation

As discussed above, the complete 2-DOF sense mode overcomes the challenges of DVA-based sense systems, such as the elimination of operational frequency scaling trade-offs [15] and the ability to independently adjust the amount of coupling between the masses. Additionally, the freedom to tailor the sense mode through this expanded mechanical design space enables a new operational method for multi-DOF gyroscopes: interchangeable operation in both robust and precision modes in a single device.

The concept of both robust and precision modes of operation is illustrated by Fig. 3 which presents a conceptual frequency response highlighting the two operational regions. Similar to previous multi-DOF devices, the robust mode corresponds to operation between the sense mode resonant frequencies, providing a wide region of relatively constant gain and phase. Precision operation, however, consists of mode-matching the drive to one of the sense mode resonant peaks. Similar to conventional devices, precision operation takes advantage of the gain achieved through resonance, allowing increasingly larger sensitivities by operating in vacuum.

Since the amount of coupling for the complete 2-DOF system is independently adjustable, it can be used to favorably shape the sense mode frequency response. The following sections will investigate how changes in the coupling parameter affect the robust mode gain when compared to a similar mismatched 1-DOF system as well as the gain ratio of the precision and robust operation.

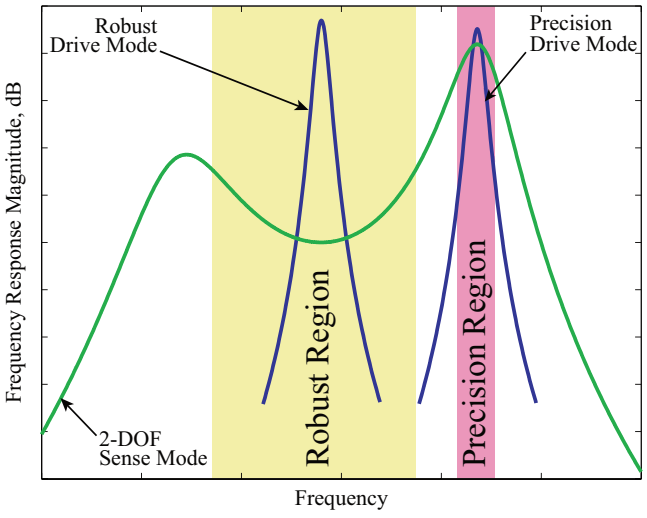

Fig. 3. Conceptual drive and sense mode frequency responses highlighting the robust and precision operational regions.

3.1. Robust mode gain advantage

In order to analytically compare robust operation using a complete 2-DOF sense mode to a conventional mismatched 1-DOF system, the mechanical gains of each are derived. Starting from the 1-DOF transfer function and taking the limit as quality factor, Q, goes to infinity gives,

$$G_{1-\mathrm{DOF}}(\omega_d) = \frac{1}{\left|2\omega_d\delta - \delta^2\right|} \tag{10}$$

which is the upper limit of mechanical gain for a conventional sense mode in terms of the frequency mismatch defined by $\delta = \omega_d - \omega_s$ where ω_d and ω_s are the drive and sense mode natural frequencies, respectively [22]. For the 2-DOF sense mode shown in Fig. 2(a), the gain can be determined from the following transfer functions

$$\frac{Y_a}{a_c} = \frac{s^2 + \omega_b^2 + \mu\omega_c^2}{s^4 + (\omega_a^2 + \omega_b^2)s^2 + \omega_a^2\omega_b^2 - \omega_c^4}, \tag{11}$$

$$\frac{Y_b}{a_c} = \frac{s^2 + \omega_a^2 + (\omega_c^2/\mu)}{s^4 + (\omega_a^2 + \omega_b^2)s^2 + \omega_a^2\omega_b^2 - \omega_c^4}, \tag{12}$$

where the input is Coriolis acceleration, $a_c = -2\Omega_z A_d\omega_d$, applied to both masses and the outputs are Y_a, the displacement of sense mass m_a, Eq. (11), and Y_b, the displacement of sense mass m_b, Eq. (12), assuming no damping and zero initial conditions. Substituting $s = i\omega_d$ into Eq. (12) and evaluating the absolute value gives,

$$G_{2-\mathrm{DOF}}(\omega_d) = \frac{1 + 4(\omega_d/\Delta)\sqrt{1-\varepsilon^2} + 16(\varepsilon/\mu)(\omega_d/\Delta)}{4\omega_d^2 - (\Delta/2)^2} \tag{13}$$

which is the mechanical gain of the complete 2-DOF sense mode assuming the smaller mass m_b is used for Coriolis detection.

Using Eq. (13), the 2-DOF gain was computed for a system with an operational frequency of 5.4 kHz and a peak spacing of 172 Hz for varying amounts of sense mode coupling, ε, and mass ratios, μ^2; these were then compared to the gain of a 1-DOF device calculated from Eq. (10) assuming a mismatch corresponding to 86 Hz (half of the 2-DOF resonant frequency separation). The results of this simulation are plotted in Fig. 4. As illustrated by the figure, the gain of the complete 2-DOF sense mode is higher for nearly all coupling values and this increase becomes larger with smaller mass ratios. Also, a maximum gain advantage exists for each mass ratio at different amounts of coupling. This maximum point can be found by

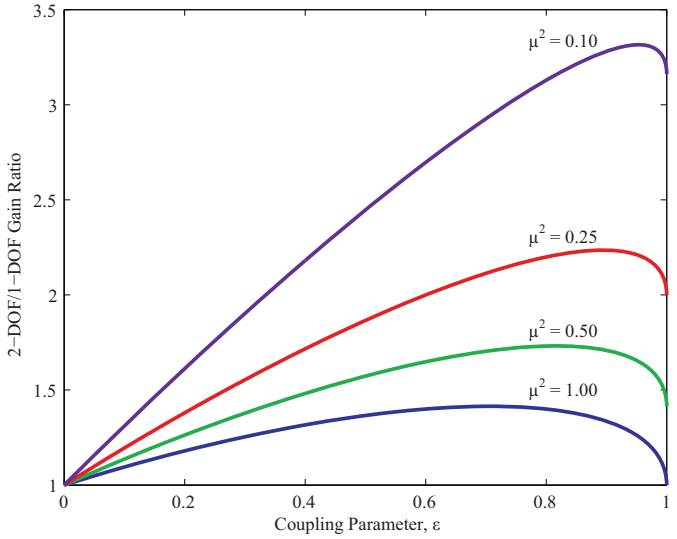

Fig. 4. Gain ratio of complete 2-DOF sense mode with peak spacing Δ to conventional 1-DOF sense mode with mismatch of $\Delta/2$.

evaluating the zero differential of the ratio,

$$\varepsilon_{\max} = \frac{1}{\sqrt{1+\mu^2}} \tag{14}$$

where $\varepsilon_{\max}$ is defined as the amount of coupling required to achieve the maximum 2-DOF gain advantage.

3.2. Gain ratio

In order to investigate the effect of coupling stiffness on the robust to precision gain ratio, frequency response simulations were performed for a complete 2-DOF system in air with constant sense mode frequency spacings for various coupling amounts. As shown in Fig. 5, the robust mode gains for all coupling amounts are essentially the same; the bandwidth, however, increases with weaker coupling due to the inclusion of the lower in-phase peak. The precision mode gains, on the other hand, change drastically with coupling starting at minimal values for maximum ($\varepsilon = 1$) and strong coupling ($0.9 < \varepsilon < 1$). Larger precision mode gain improvement for atmospheric operation is obtained with decreasing coupling stiff-

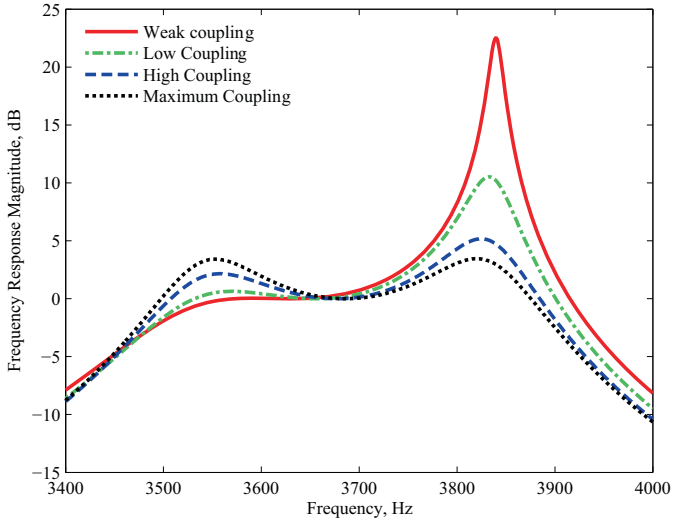

Fig. 5. Simulated sense mode frequency responses revealing the design trade-offs: weaker coupling results in larger precision mode gain for atmospheric pressure.

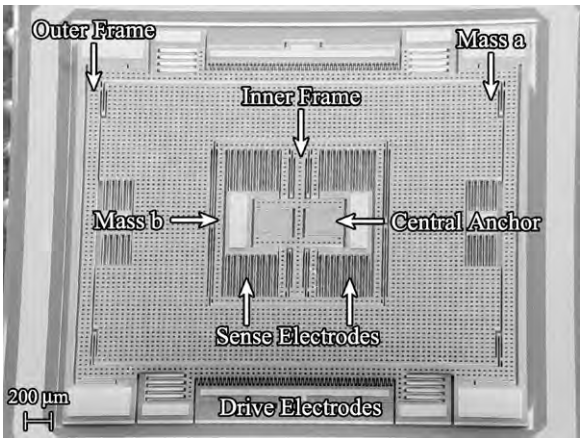

Fig. 6. SEM image of fabricated gyroscope prototype.

ness resulting in an increase of more than 20 dB versus the robust mode for weakly coupled systems ($\varepsilon < 0.3$). Thus, weak coupling is ideal for purely atmospheric operation as it maximizes the precision mode gain improvement.

4. Experimental characterization

Prototypes of the proposed gyroscope concept used for the experimental characterization presented below were fabricated using an in-house, wafer scale silicon-on-insulator process with a conductive 50 μm device layer and a 5 μm buried oxide. The minimum feature size of the overall process used to define the capacitive gaps was 5 μm. The perforated structures were released using a timed hydrofluoric (HF) acid bath followed by dicing, packaging, and wire bonding. A scanning electron micrograph (SEM) of a fabricated prototype is presented in Fig. 6.

Imperfections arising due to the fabrication process are a common problem for micromachined resonant devices, especially gyroscopes, where the resonant frequencies are strongly dependent upon the geometric dimensions of relatively thin suspension elements. This can cause a deviation of the drive and sense mode resonant frequencies from the intended values and for conventional silicon gyroscopes, the scattering can be on the order of 100 Hz [23]. To compensate for these effects, post fabrication mechanical trimming is typically employed to adjust resonant frequencies [24] which ultimately increases the total cost per sensor. Detailed numerical simulations of vibratory gyroscopes with coupled sense mode designs show an order of magnitude improvement in sensitivity of the scale factor to the variations in the fabrication process critical dimension [25], thereby eliminating the need for trimming.

4.1. Sense mode frequency responses

In order to investigate the robust mode gain advantage versus a conventional 1-DOF mismatched device, two sense mode systems were designed and fabricated. The first was a complete 2-DOF system with masses m_a and m_b while the second was identical to the first except the masses were fused to form a 1-DOF system with the same total mass, $m_a + m_b$. Frequency responses were experimentally obtained for both systems in air using equivalent electrostatic forcing and are presented in Fig. 7. As indicated by the figure, the robust mode gain of the complete 2-DOF system is over 5 dB higher than the gain of the 1-DOF system mode-mismatched by half the resonant frequency spacing, thereby demonstrating the advantage predicted in Fig. 4.

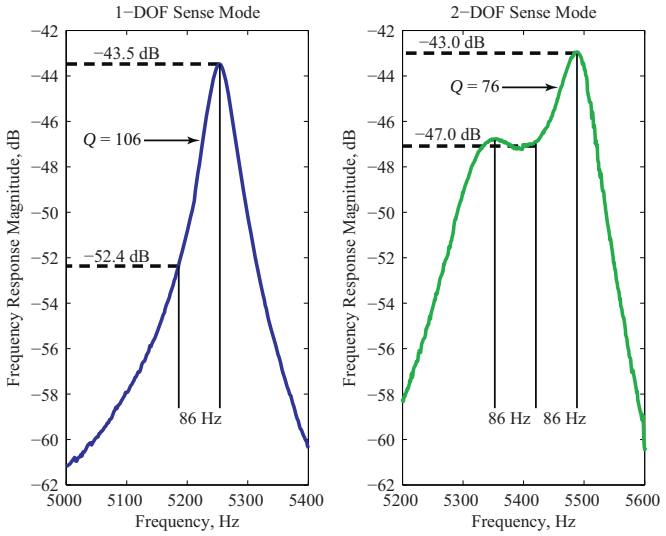

Fig. 7. Experimental comparison of similar 1- and 2-DOF sense modes systems demonstrating the advantages of both robust and precision operation.

An additional gain-bandwidth advantage is revealed in Fig. 7 for precision operation. While the absolute gains are essentially the same, the effective Q factor of the 2-DOF resonant peak is 76 versus the slightly higher Q of 106 for the 1-DOF system despite the same damping conditions. Therefore, the precision mode of operation can provide the equivalent mechanical gain of a conventional 1-DOF system with a lower effective quality factor and thus, larger bandwidth.

The precision to robust gain ratio was examined using several different sense mode systems with varying degrees of coupling between the masses. Experimental frequency responses are presented in Fig. 8 for sense modes systems with strong and weak coupling in both air and 1 mTorr vacuum. As expected from the previous analysis and simulations in Fig. 5, the low coupling system provides a higher precision mode gain improvement in air (10 dB versus 7 dB) versus the 240 Hz wide robust gain regions. On the other hand, the system with a high coupling stiffness provides the larger precision mode improvement of more than 40 dB versus the robust region in vacuum. Additionally, the robust region

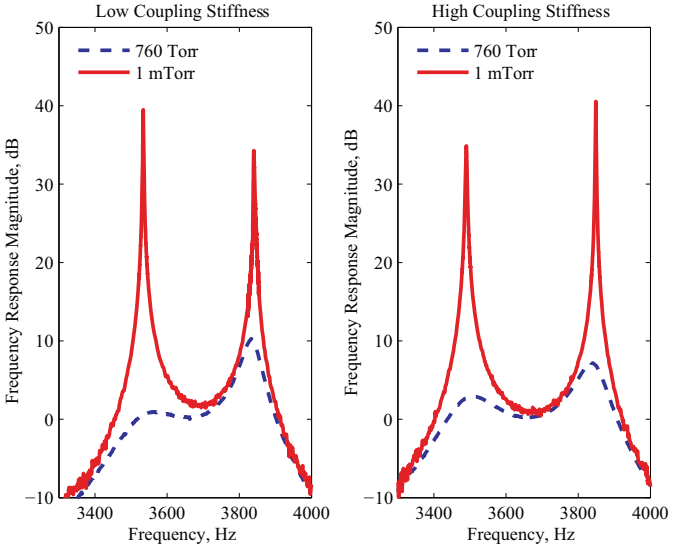

Fig. 8. Sense mode frequency responses in air and vacuum of fabricated gyroscope prototypes with high and low coupling stiffnesses.

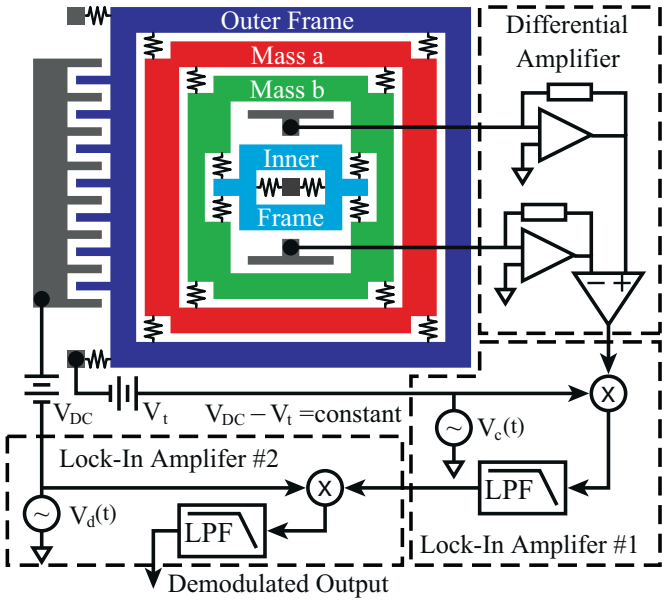

Fig. 9. Schematic of the actuation and detection architecture used for the experimental characterization of the gyroscope.

of the strongly coupled sense mode is unaffected as the pressure is decreased; for the low stiffness system, however, this is not the case since the robust region contained the lower, in-phase peak in air, which changes dramatically in vacuum.

4.2. Angular rate characterization

The fabricated prototype was characterized using constant angular rates for both robust and precision modes. The sections below detail the biasing used for the experiment, Section 4.2.1, the method of mode tuning for switching between the operational modes, Section 4.2.2, and finally, a scale factor comparison in Section 4.2.3.

4.2.1. Biasing scheme

Fig. 9 presents a schematic of the actuation and detection scheme used for the angular rate experimental characterization. For drive mode actuation, an AC driving voltage, $V_d(t)$ plus a DC potential, V_{DC} was applied to the fixed electrodes while a high frequency AC carrier voltage, $V_c(t)$, plus a sense mode tuning voltage, V_t was applied to the mobile mass. In order to maintain a constant driving amplitude, the total DC driving potential, $V_{DC} - V_t$, was fixed during sense mode tuning experiments.

In the sense mode, a differential detection scheme using cascaded trans-impedance and instrumentation amplifiers was used to pick up the motion of mass m_b. The differential signal was then demodulated at the carrier frequency followed by a second demodulation at the drive frequency using AMETEK Model 7265 Lock-In Amplifiers. The use of the high frequency carrier allows for the separation of useful sense signals from the drive feed-through [26].

4.2.2. Mode-matching

The fabricated prototype used in the experimental characterization was designed with the drive mode natural frequency of 5.44 kHz between the lower and higher sense mode resonances of 5.2 and 5.6 kHz, respectively. Therefore, mode-matching for the presented device required electrostatic tuning of the sense mode in order to match the higher anti-phase resonant frequency to the drive. By adjusting the DC tuning voltage, V_t applied to the mass, the sense mode resonant frequencies are shifted down in frequency

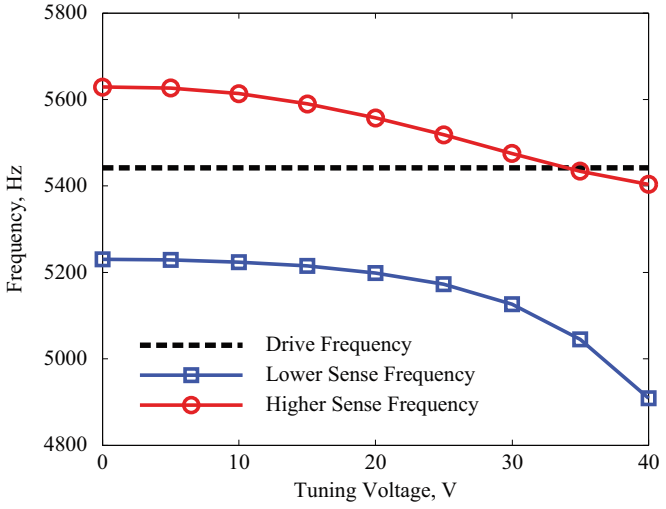

Fig. 10. Sense mode resonant frequencies versus applied tuning voltage demonstrating the ability to switch between robust and precision modes.

as shown in Fig. 10. Continuing to increase the voltage causes both sense mode frequencies to shift until the higher one crosses the drive mode at approximately 35 V.

While the sense mode tuning curves indicate that the device can be mode-matched, it does not ensure precise matching is achieved. The zero rate output of the gyroscope (or quadrature), however, can be monitored for a maximum output indicating that the drive and sense frequencies are equal [27]. The quadrature output in dB versus tuning voltage is presented in Fig. 11 for the device operated in 5.6 Torr vacuum. For low tuning voltages (0–15 V), the drive mode is in the robust operational region between the peaks. As the voltage is increased, the quadrature signal reaches a maximum at 34 V indicating a mode-matched condition; further increases in tuning voltage, however, results in a decreased output signal.

4.2.3. Scale factor comparison

To verify both operational modes, the device was characterized in atmospheric pressure at constant angular rates using an Ideal Aerosmith 1291BR rate table and the results of the experiment are presented in Fig. 12. The actuation and detection scheme shown in Fig. 9 was used with tuning voltages of 0 V and 34 V for robust and

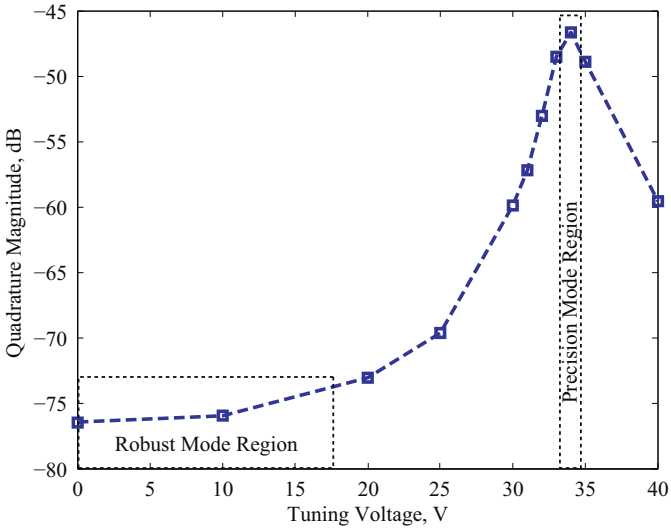

Fig. 11. Zero rate output of the gyroscope as a function of tuning voltage indicating the switch between robust and precision modes.

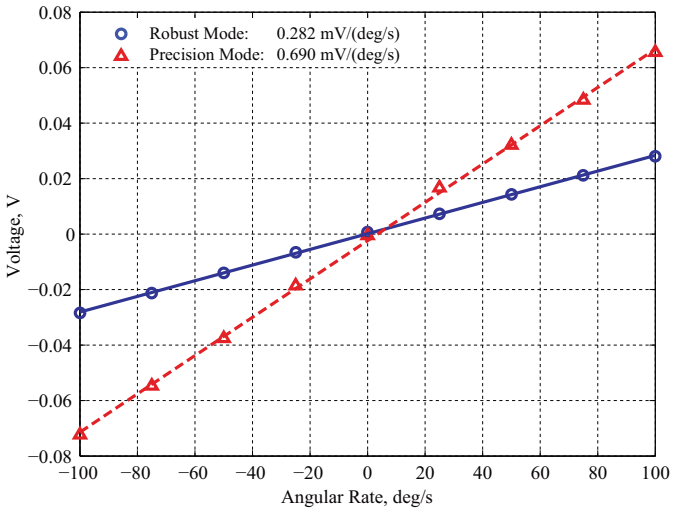

Fig. 12. Constant angular rate characterization for both robust and precision modes in air.

precision modes, respectively, while the total driving voltage was kept constant. For robust operation, the experimentally obtained scale factor was 0.282 mV/°/s while for precision operation it was 0.690 mV/°/s. Thus, precision mode resulted in a 2.4 times improvement of scale factor at atmospheric pressure; for operation at 1 mTorr vacuum, however, a possible improvement of 40 dB can be obtained for precision mode while leaving the robust mode unaffected.

5. Conclusions

A new *z*-axis vibratory MEMS gyroscope concept with a complete 2-DOF sense mode was presented. The device, unlike previous multi-DOF designs based on dynamic vibration absorber systems, allows for the specification of the sense mode frequency spacing and coupling independent of the operational frequency. This is accomplished through the addition of a second, inner decoupling frame ensuring *x*–*y* symmetry without a bidirectional flexure.

Additionally, a new operational method was introduced allowing interchangeable operation in either precision or robust modes. The robust mode corresponds to operation between the 2-DOF sense mode resonant frequencies and was analytically and experimentally shown to provide a gain advantage over a similar 1-DOF system operated with a mismatch. Precision operation relies on matching the drive to one of the sense mode resonant frequencies which was revealed to have a gain-bandwidth advantage over a conventional sense mode.

The trade-offs associated with the amount of coupling between the sense masses were investigated. For atmospheric pressure, weakly coupled systems are desirable due to the larger achievable precision mode gain improvements (over 20 dB); for vacuum operation, however, the high coupling stiffness system results in the larger precision mode gain (over 40 dB) while leaving the robust region relatively unaffected. In the robust mode of operation, uncompensated temperature coefficients of bias and scale factor have been shown to be on the order of 300 (°/h)/°C and 350 ppm/°C, respectively, due to the robustness of the coupled sense mode [16]. In the precision mode, temperature robustness and bandwidth of the gyroscope are traded for up to 100 times improvement in the mechanical sensitivity and, correspondingly, the Angle Random Walk (ARW). Finally, an experimental rate characterization of a silicon-on-insulator prototype was performed for both robust and precision modes in air revealing a 2.4 times scale factor improvement which can be increased 40 dB for 1 mTorr operation.

6. Acknowledgements

This work was supported by the National Science Foundation Grant CMS-0409923, Systron Donner Automotive contract BEI-36974, UC Discovery program ELE04-10202, and Naval Surface Warfare Center contract N00178-08-C1014. The authors would like to acknowledge University of California, Irvine Integrated Nanosystems Research Facility (INRF) for assistance with the fabrication of prototypes and the Carl Zeiss Center of Excellence for use of the Ultra 55 SEM. The gyroscopes were designed and characterized at the MicroSystems Laboratory, University of California, Irvine.

References

[1] A.M. Shkel, Type I and Type II micromachined vibratory gyroscopes, in: Proceedings of the IEEE/ION PLANS 2006, San Diego, CA, USA, 2006, pp. 586–593.
[2] N. Yazdi, F. Ayazi, K. Najafi, Micromachined inertial sensors, in: Proceedings of the IEEE, 1998, pp. 1640–1659.
[3] M. Weinberg, A. Kourepenis, Error sources in in-plane silicon tuning-fork MEMS gyroscopes, IEEE/ASME Journal of Microelectromechanical Systems 15 (3) (2006) 479–491.
[4] R. Neul, U.-M. Gomez, K. Kehr, W. Bauer, J. Classen, C. Doring, E. Esch, S. Gotz, J. Hauer, B. Kuhlmann, C. Lang, M. Veith, R. Willig, Micromachined angular rate sensors for automotive applications, IEEE Sensors Journal 7 (2) (2007) 302–309.
[5] J.A. Geen, S.J. Sherman, J.F. Chang, S.R. Lewis, Single-chip surface micromachined integrated gyroscope with 50 deg/h allan deviation, IEEE Journal of Solid-State Circuits 37 (12) (2002) 1860–1866.
[6] J. Geen, Very low cost gyroscopes, in: Proceedings of the IEEE Sensors, Irvine, CA, USA, 2005, pp. 537–540.
[7] U.-M. Gomez, B. Kuhlmann, J. Classen, W. Bauer, C. Lang, M. Veith, E. Esch, J. Frey, F. Grabmaier, K. Offterdinger, T. Raab, H.-J. Faisst, R. Willig, R. Neul, New surface micromachined angular rate sensor for vehicle stabilizing systems in automotive applications, in: Proceedings of the International Conference on Solid-State Sensors, Actuators and Microsystems (TRANSDUCERS '05), Seoul, Korea, 2005, pp. 184–187.
[8] A. Madni, L. Costlow, S. Knowles, Common design techniques for BEI gyrochip quartz rate sensors for both automotive and aerospace/defense markets, IEEE Sensors Journal 3 (5) (2003) 569–578.
[9] R. Neul, U. Gomez, K. Kehr, W. Bauer, J. Classen, C. Doring, E. Esch, S. Gotz, J. Hauer, B. Kuhlmann, C. Lang, M. Veith, R. Willig, Micromachined gyros for automotive applications, in: Proceedings of the IEEE Sensors 2005, Irvine, CA, USA, 2005, pp. 527–530.
[10] C. Acar, A. Shkel, Inherently robust micromachined gyroscopes with 2-DOF sense-mode oscillator, IEEE/ASME Journal of Microelectromechanical Systems 15 (2) (2006) 380–387.
[11] A.R. Schofield, A.A. Trusov, C. Acar, A.M. Shkel, Anti-phase driven rate gyroscope with multi-degree of freedom sense mode, in: Proceedings of the 14th International Conference on Solid-State Sensors, Actuators and Microsystems (TRANSDUCERS '07), Lyon, France, 2007, pp. 1199–1202.
[12] A.R. Schofield, A.A. Trusov, A.M. Shkel, Multi-degree of freedom tuning fork gyroscope demonstrating shock rejection, in: Proceedings of the IEEE Sensors, Atlanta, GA, USA, 2007, pp. 120–123.
[13] S. Alper, K. Azgin, T. Akin, A high-performance silicon-on-insulator MEMS gyroscope operating at atmospheric pressure, Sensors and Actuators A: Physical 135 (1) (2007) 34–42.
[14] W.-T. Sung, S. Sung, J.G. Lee, T. Kang, Design and performance test of a MEMS vibratory gyroscope with a novel AGC force rebalance control, Journal of Micromechanics and Microengineering 17 (10) (2007) 1939–1948.
[15] A.R. Schofield, A.A. Trusov, A.M. Shkel, Effects of operational frequency scaling in multi-degree of freedom mems gyroscopes, IEEE Sensors Journal 8 (10) (2008) 1672–1680.
[16] A.A. Trusov, A.R. Schofield, A.M. Shkel, Performance characterization of a new temperature-robust gain-bandwidth improved MEMS gyroscope operated in air, Sensors and Actuators A: Physical 155 (1) (2009) 16–22.
[17] K. Sahin, E. Sahin, S.E. Alper, T. Akin, A wide-bandwidth and high-sensitivity robust microgyroscope, Journal of Micromechanics and Microengineering 19 (2009), p. 074004 (8 pp.).
[18] M.S. Kranz, G.K. Fedder, Micromechanical Vibratory Rate Gyroscope Fabricated in Conventional CMOS, Symposium Gyro Technology, Stuttgart, Germany, 1997, pp. 3.0–3.8.
[19] A.R. Schofield, A.A. Trusov, A.M. Shkel, Micromachined gyroscope design allowing for both robust wide-bandwith and precision mode-matched operation, in: Proceedings of the IEEE Sensors, Lecce, Italy, 2008, pp. 654–657.
[20] A.R. Schofield, A.A. Trusov, A.M. Shkel, Design trade-offs of micromachined gyroscope concept allowing interchangeable operation in both robust and precision modes, in: Proceedings of the International Solid-State Sensors, Actuators and Microsystems Conference (TRANSDUCERS 2009), Denver, CO, USA, 2009, pp. 1952–1955.

[21] J.P. Den Hartog, Mechanical Vibrations, Dover Publications, New York, NY, 1985.
[22] J. Söderkvist, Micromachined gyroscopes, Sensors and Actuators A: Physical 43 (1–3) (1994) 65–71.
[23] X. Chen, W. Cui, W. Xue, Process modeling and device-package simulation for optimization of MEMS gyroscopes, Computer-Aided Design and Applications 6 (3) (2009) 375–386.
[24] A. Madni, L. Costlow, A third generation, highly monitored, micromachined quartz rate sensor for safety-critical vehicle stability control, in: Proceedings of the IEEE Aerospace Conference, 2001, pp. 2523–2534.
[25] W. Cui, X. Chen, W. Xue, Design optimization for a non-resonant MEMS gyroscope, in: Proceedings of the 2009 ASME International Mechanical Engineering Congress and Exposition (ASME IMECE 2009), Lake Buena Vista, FL, 2009.
[26] A.A. Trusov, A.M. Shkel, Capacitive detection in resonant MEMS with arbitrary amplitude of motion, Journal of Micromechanics and Microengineering 17 (8) (2007) 1583–1592.
[27] A. Sharma, M. Zaman, F. Ayazi, A smart angular rate sensor system, in: Proceedings of the IEEE Sensors, Atlanta, GA, USA, 2007, pp. 1116–1119.

Biographies

Adam R. Schofield received the B.S. degree in mechanical engineering summa cum laude with honors and the M.S. degree in mechanical engineering supported by an Ohio Space Grant Fellowship from the University of Dayton, Dayton, OH, in 2002 and 2005, respectively. In 2009, he received the Ph.D. degree in mechanical and aerospace engineering from the University of California, Irvine where his research focused on the design, fabrication, packaging, and characterization of MEMS inertial sensors. Currently, Dr. Schofield is a Senior Scientist at System Planning Corporation (SPC) in Arlington, VA where he provides technical support to the Microsystems Technology Office (MTO) of the Defense Advanced Research Projects Agency (DARPA). Dr. Schofield was awarded the Class of 2002 Award for Outstanding Mechanical Engineering Achievement by the University of Dayton and is a member of the Institute of Electrical and Electronics Engineers (IEEE), the American Society of Mechanical Engineers (ASME), as well as the Tau Beta Pi, Pi Tau Sigma, and Golden Key Honor Societies.

Alexander A. Trusov received the diploma in applied mathematics and mechanics from the Moscow State University, Moscow, Russia in 2004 and the M.S. and Ph.D. degrees in mechanical and aerospace engineering from the University of California, Irvine in 2006 and 2009, respectively. He is currently a project scientist at the UC Irvine MicroSystems laboratory where he is leading several government funded programs on high performance inertial microsystems. Dr. Trusov's research interests include design, modeling, fabrication, and vacuum packaging of micromachined inertial systems, design of characterization experiments, and statistical data processing and analysis. Dr. Trusov has published over 25 journal and international conference papers on MEMS inertial sensors, has 6 patents pending, and serves as a reviewer for major journals in the fields of MEMS and sensors. He is a member of the American Society of Mechanical Engineers (ASME), and the Institute of the Institute of Electrical and Electronics Engineers (IEEE).

Andrei M. Shkel received the diploma degree (with excellence) in mechanics and mathematics from Moscow State University, Moscow, Russia, in 1991, and the Ph.D. degree in mechanical engineering from the University of Wisconsin, Madison, in 1997. He is a Program Manager in the Microsystems Technology Office of the Defense Advanced Research Projects Agency (DARPA), Arlington, VA; he is serving in this capacity while on leave from his faculty position as a professor in the Department of Mechanical and Aerospace Engineering at University of California, Irvine, CA, where he is also the Director of the UCI Microsystems Laboratory. He is the holder of thirteen U.S. and international patents. His professional interests are reflected in more than 120 publications. He is an editor of IEEE JMEMS. Dr. Shkel is the recipient of the 2010 IEEE Sensors Council Technical Achievement Award, the 2006 UCI HSSOE Research Award, the 2005 NSF CAREER Award, and the 2002 George E. Brown, Jr., Award.